# Page Proof Instructions and Queries

**Journal Title:** Journal of Cerebral Blood Flow & Metabolism (JCB)

**Article Number:** 615132

Greetings, and thank you for publishing with SAGE. We have prepared this page proof for your review. Please respond to each of the below queries by digitally marking this PDF using Adobe Reader.

Click "Comment" in the upper right corner of Adobe Reader to access the mark-up tools as follows:

For textual edits, please use the "Annotations" tools. Please refrain from using the two tools crossed out below, as data loss can occur when using these tools.

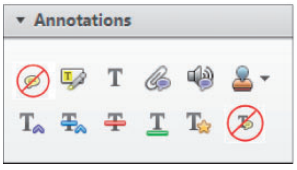


For formatting requests, questions, or other complicated changes, please insert a comment using "Drawing Markups."


Detailed annotation guidelines can be viewed at: http://www.sagepub.com/repository/binaries/pdfs/AnnotationGuidelines.pdf
Adobe Reader can be downloaded (free) at: http://www.adobe.com/products/reader.html.

| No. | Query |
|---|---|
| | Please confirm that all author information, including names, affiliations, sequence, and contact details, is correct. |
| | Please review the entire document for typographical errors, mathematical errors, and any other necessary corrections; check headings, tables, and figures. |
| | Please confirm that the Funding and Conflict of Interest statements are accurate. |
| | Please ensure that you have obtained and enclosed all necessary permissions for the reproduction of artistic works, (e.g. illustrations, photographs, charts, maps, other visual material, etc.) not owned by yourself. Please refer to your publishing agreement for further information. |
| | Please note that this proof represents your final opportunity to review your article prior to publication, so please do send all of your changes now. |

*Original Article*

JCBFM

Journal of Cerebral Blood Flow & Metabolism
0(00) 1–16

DOI: 10.1177/0271678X15615132
jcbfm.sagepub.com

SAGE

# Synaptosomal bioenergetic defects are associated with cognitive impairment in a transgenic rat model of early Alzheimer's disease

**Pamela V Martino Adami[1], Celia Quijano[2], Natalia Magnani[3], Pablo Galeano[1,4], Pablo Evelson[3], Adriana Cassina[2], Sonia Do Carmo[5], María C Leal[6], Eduardo M Castaño[1], A Claudio Cuello[5] and Laura Morelli[1]**

## Abstract

Synaptic bioenergetic deficiencies may be associated with early Alzheimer's disease (AD). To explore this concept, we assessed pre-synaptic mitochondrial function in hemizygous (+/−)TgMcGill-R-Thy1-APP rats. The low burden of Aβ and the wide array of behavioral and cognitive impairments described in 6-month-old hemizygous TgMcGill-R-Thy1-APP rats (Tg(+/−)) support their use to investigate synaptic bioenergetics deficiencies described in subjects with early Alzheimer's disease (AD). In this report, we show that pre-synaptic mitochondria from Tg(+/−) rats evidence a decreased respiratory control ratio and spare respiratory capacity associated with deficits in complex I enzymatic activity. Cognitive impairments were prevented and bioenergetic deficits partially reversed when Tg(+/−) rats were fed a nutritionally complete diet from weaning to 6-month-old supplemented with pyrroloquinoline quinone, a mitochondrial biogenesis stimulator with antioxidant and neuroprotective effects. These results provide evidence that, as described in AD brain and not proven in Tg mice models with AD-like phenotype, the mitochondrial bioenergetic capacity of synaptosomes is not conserved in the Tg(+/−) rats. This animal model may be suitable for understanding the basic biochemical mechanisms involved in early AD.

## Keywords

Amyloid β, early-Alzheimer, hippocampal bioenergetics status, neurodegeneration, synaptosomes

Received 18 March 2015; Revised 5 October 2015; Accepted 8 October 2015

## Introduction

The amyloid hypothesis proposes that high levels of amyloid β (Aβ) culminate in neuronal damage and Alzheimer's disease (AD).[1] Positron emission tomography (PET) with 18F-fluoro-2-deoxy-D-glucose has shown that in AD, glucose metabolism changes over time indicating that it could serve as a predictive marker of neurodegeneration.[2] Brain hypometabolism in AD cases is consistent with a decreased metabolic demand[3] which may be partially explained by a lower expression of mitochondrial genes in specific brain areas.[4] Mitochondrial accumulation of Aβ (*mit*Aβ)[5] is a pathogenic event only described by ultrastructural analysis in AD brains and in transgenic (Tg) mice models of AD. *Mit*Aβ seems to induce mitochondrial

[1]Laboratory of Amyloidosis and Neurodegeneration, Fundación Instituto Leloir-IIBBA-CONICET, Buenos Aires, Argentina
[2]Department of Biochemistry and Center for Free Radical and Biomedical Research, Facultad de Medicina, Universidad de la República, Montevideo, Uruguay
[3]IBIMOL-UBA-CONICET, Facultad de Farmacia y Bioquímica, Universidad de Buenos Aires, Buenos Aires, Argentina
[4]ININCA- UBA-CONICET, Facultad de Medicina, Universidad de Buenos Aires, Buenos Aires, Argentina
[5]Department of Pharmacology and Therapeutics, McGill University, Montreal, Quebec, Canada
[6]Laboratory of Protective and Regenerative Therapies of the CNS, Fundación Instituto Leloir-IIBBA-CONICET, Buenos Aires, Argentina

**Corresponding author:**
Laura Morelli, Laboratory of Amyloidosis and Neurodegeneration, Fundación Instituto Leloir-IIBBA CONICET, Ave. Patricias Argentinas 435. C1405BWE. Buenos Aires, Argentina.
Email: lmorelli@leloir.org.ar

dysfunction, one of the earliest and most prominent alterations in AD brain.[6] Recently, we showed that the catabolism of *mit*Aβ[7] is pharmacologically modulated by pyrroloquinoline quinone (PQQ). PQQ is an anionic, water-soluble compound that has been shown to be an essential nutrient in mice.[8] PQQ can cross the blood–brain barrier[9] and has neuroprotective effects.[10] In several AD mouse models, mitochondria function has been studied, overall showing deficits in respiration and changes in morphology and transport.[11,12] In addition to Aβ accumulation and mitochondrial dysfunction, it was proposed that bioenergetic defects in large nerve terminals (synaptosomes) are associated with progression of AD. However, this hypothesis has not been proven in commonly used Tg mice models with a complete amyloid phenotype (including dense fibrillar extracellular Aβ deposition) characteristic of late AD.[13] Recently, novel murine models of AD pathology have been developed including TgMcGill-R-Thy1-APP rats. Homozygous animals display the full amyloid pathology (mature plaques, dystrophic neurites and peri-plaque inflammation) while hemizygous (Tg+/−) rats show intra-neuronal accumulation of Aβ (iAβ) throughout their entire life and occasionally generate amyloid plaques. Moreover, they show a wide array of behavioral and cognitive impairments at pre-plaque stages.[14] To determine whether Tg(+/−) rats imitate the hippocampal bioenergetic defects observed in early AD brain, brains of 6-month-old Tg(+/−) and wild type (WT) controls were analyzed. By *in situ* respirometry, we detected in Tg(+/−) decrements in synaptosomal respiratory control ratio and spare respiratory capacity as compared to WT rats in agreement with a reduced mitochondrial complex I enzymatic activity. By contrast, neither complex II nor α-ketoglutarate dehydrogenase complex (α-KGDHC) activities showed significant differences between Tg(+/−) and WT rats. Cognitive defects characteristic of these animals at 6 months of age were not related to any ultrastructural change of the hippocampal CA1 region but were prevented, and mitochondrial function partially recovered when Tg(+/−) rats were fed a nutritionally complete diet supplemented with PQQ. These findings suggest that at 6 months of age Tg(+/−) rats display core behavioral features of early AD possibly due to initial bioenergetic alterations of hippocampal synaptosomes and provide further validation for its usage as a valuable tool to understand the underlying early mechanisms of this neurodegenerative disorder.

## Materials and methods

### Ethical statements

The study was carried out in strict accordance with the ARRIVE (Animal Research: Reporting of *In Vivo* Experiments) and the OLAW-NIH (Office Laboratory Animal Welfare) guidelines. The protocol was approved by the local Animal Care Committee of Fundación Instituto Leloir (FIL) Assurance# A5168-01.

### Reagents

BioPQQ™ (pyrroloquinoline quinone disodium salt) was kindly provided by Mitsubishi Gas Chemical Company (Tokyo, Japan). Diamidino-2-phenylindole (DAPI) was purchased from Life Technologies. Oligomycin, carbonyl cyanide m-chlorophenyl hydrazone (m-CCCP), carbonylcyanide p-trifluoromethoxyphenylhydrazone (FCCP), 2,6-dichlorophenol indophenol (DCPIP), antimycin, horseradish peroxidase, superoxide dismutase, scopoletin, D-luciferin, luciferase, Ficoll, digitonin, dimethyl sulfoxide (DMSO), polyethylenimine, β-nicotinamide adenine dinucleotide ~~phosphate~~ sodium salt ~~hydrate~~ ($NAD^+$) and coenzyme A sodium salt hydrate (CoA) were from Sigma-Aldrich. Thiamine pyrophosphate (TPP) was from Merck. Fetal calf serum (FCS) was from Natocor.

### Animals and nutritional protocols

Hemizygous transgenic McGill-R-Thy1-APP (Tg(+/−)) rats harboring the human APP751 transgene with the Swedish and Indiana mutation under the control of the murine Thy1.2 promoter were generated using HsdBrI:WH Wistar strain.[14] Animals were provided to Fundación Instituto Leloir (FIL) by The Royal Institution for the Advancement of Learning/McGill University, Montreal, Quebec (Canada). An in-house colony was established at FIL as previously described.[15] Tg(+/−) rats and littermates wild type (WT) controls were maintained in polycarbonate cages in a temperature-controlled animal facility with a 12-h dark/light cycle and allowed to consume standard diet and water ad libitum. For separate experiments, BioPQQ was added to water at 2 mg/kg.[16] Rats were fed with BioPQQ diet from weaning up to 6 months of age. Thirty days before the end of the experiment, 5-month-old animals received a supplement of BioPQQ (20 mg/kg/day) given once a day via oral gavage (10 mL/kg body weight). Mixed gender (approximately half male and half females) was used for hippocampal bioenergetic assessment. By contrast, for behavioral performance, only male rats were used to avoid any potential effects of female estrus cycle on this paradigm.

### Behavioral and cognitive testing

Neurological reflexes, exploratory activity, emotional behavior, recognition and spatial working and

reference memory were assessed as previously reported.[15] Description of each test is given online in the Supplementary Information (SI).

### Mitochondrial oxygen consumption studies

Subcellular fractions enriched in mitochondria were obtained from hippocampal homogenates of 6-month-old rats by differential centrifugation following standard procedures.[17] Oxygen consumption studies to evaluate mitochondrial respiration were performed using high-resolution respirometry (Hansatech Oxygraph, Hansatech Instruments Ltd, Norfolk, UK).[18] Mitochondria were incubated in respiration buffer supplemented with 6 mM malate and glutamate or 7 mM succinate as substrates. An initial rest state respiration in the absence of ADP (state 4) was established under these conditions, which was then switched to active state respiration (state 3) by the addition of 1 mM ADP. State 3 is defined as the maximum physiological ATP production rate and $O_2$ consumption and it is considered as ~~that~~ responsible for the physiological $O_2$ consumption. Results are expressed as ng-at O/min/mg protein.

### Mitochondrial oxidative metabolism

Hydrogen peroxide ($H_2O_2$) generation was assessed in hippocampal mitochondria of 6-month-old rats by the scopoletin-horseradish peroxidase method, following the decrease in fluorescence intensity at 365–450 nm ($\lambda_{exc}$–$\lambda_{em}$) at 30°C.[19] $H_2O_2$ production was triggered by the addition of 6 mM malate and 6 mM glutamate. Results were expressed as nmol $H_2O_2$/min/mg protein. Oxidative damage to phospholipids was evaluated in hippocampal mitochondria by measuring thiobarbituric acid reactive substances (TBARS) with a fluorometric assay.[20] Results are expressed as nmol TBARS/mg protein.

### Synaptosomes isolation, biochemical and microscopical characterization

Six-month-old WT and Tg(+/−) rats were decapitated and brains were quickly removed. Hippocampi were dissected in ice-cold MSTE buffer (0.23 M mannitol, 0.07 M sucrose, 10 mM Tris-HCl, 1 mM EDTA, pH 7.4) and homogenized with a manual Teflon glass homogenizer in 2 mL of MSTE. Homogenates were centrifuged at $600 \times g$ for 10 min to discard cell debris and nuclei and supernatants were centrifuged again at $8000 \times g$ to obtain crude mitochondrial pellets. Pellets were washed, resuspended in 2 mL of MSTE, and layered on 13%, 8%, and 3% Ficoll step-gradients. Gradients were centrifuged at $11{,}500 \times g$ for 30 min. The fraction at 8% was recovered, diluted in HBS buffer (20 mM HEPES, 10 mM D-glucose, 1 mM $MgCl_2$, 5 mM KCl, 140 mM NaCl, 1.2 mM $Na_2HPO_4$, 5 mM $NaHCO_3$, pH 7.4), and centrifuged at $11{,}500 \times g$ for 10 min to obtain a synaptosomal pellet. Synaptosomes were resuspended in 600 µL of HBS containing 10% FCS, 10% DMSO and cryopreserved at liquid nitrogen until use. All procedures were carried out at 0–2°C. Biochemical and microscopical characterization of synaptosomes is detailed online in Supplementary Information.

### ATP production rate

A chemiluminescence assay based on the luciferin–luciferase system was used to evaluate ATP production rate in hippocampal mitochondria of 6-month-old rats or in freshly purified and permeabilized (0.01% digitonin) synaptosomes. Methodology is described online in the Supplementary Information. The number of phosphorylated ADP molecules per oxygen atom (P/O ratio) was calculated as the mean value of mitochondrial ATP production/mean value of state 3 oxygen consumption rate.

### Synaptosomal oxygen consumption rate and ~~E~~extracellular acidification rate assays

Synaptosomes were rapidly thawed, diluted in HBS and centrifuged at $11{,}500 \times g$ for 5 min. Pellets were resuspended in HBS and protein concentration was determined with a Pierce BCA Protein Assay Kit (Thermo Scientific). Twenty-five µg of protein were plated into 20 wells of a XF$^e$24 V7 cell culture microplate (Seahorse Bioscience) previously coated with polyethyleneimine (1:15 000 dilution of a 50% v/v stock) and centrifuged at $3600 \times g$ for 1 h at 4°C to attach synaptosomes. HBS medium was replaced with 600 µL of incubation medium (3.5 mM KCl, 120 mM NaCl, 1.3 mM $CaCl_2$, 0.4 mM $KH_2PO_4$, 1.2 mM $Na_2SO_4$, 2 mM $MgSO_4$, 15 mM D-glucose with or without 10 mM pyruvate, 4 mg/mL BSA, pH 7.4). Plates were kept at 37°C for 20 min and loaded into the Seahorse XF$^e$24 extracellular flux analyzer following the manufacturer's instructions. All experiments were performed at 37°C. Baseline measurements of OCR and ECAR were performed at the beginning of the assay, and these were followed by the sequential addition of an ATP synthase inhibitor (oligomycin), an uncoupler of oxidative phosphorylation (FCCP), and an inhibitor of complex III (antimycin). Generally, four baseline measurements and three response rates (after the addition of a compound) were measured and the average of these rates used for data analysis. Synaptosomes were first titrated with 1–4 µM of FCCP and 1–5 µM of oligomycin. One µM

FCCP gave the maximum oxygen consumption rate and 5 μM oligomycin rendered the maximum inhibition of the oxygen consumption rate, so these concentrations were used for the experiments. Non-mitochondrial oxygen consumption rate was determined after the addition of 5 μM antimycin (antimycin resistant OCR), and substracted from all other values before calculation of the respiratory parameters as previously described.[13] Respiratory parameters are obtained as follows: *basal respiration*, baseline OCR; *respiration driving proton leak*, OCR after the addition of 5 μM oligomycin; *respiration ~~diving~~ ATP synthesis*, basal respiration – respiration driving proton leak; *maximum respiration*, OCR after the addition of 1 μM FCCP; *respiratory control ratio (RCR)*, maximum respiration/respiration driving proton leak; *spare respiratory capacity*, maximum respiration – basal respiration as previously described[21]; *coupling efficiency*, respiration driving ATP synthesis/basal respiration.

### Enzyme assays

Methodology to assess mitochondrial complex I, complex II, citrate synthase and α-ketoglutarate dehydrogenase enzyme complex (α-KGDHC) activities is described online in the Supplementary Information.

### Quantitation of synaptic density and mitochondrial morphology by transmission electron microscopy

Methodology to estimate the synaptic density and the size and shape of mitochondria is described online in Supplementary Information.

### Estimation of iAβ levels and oxidative damage in the hippocampus affected by iAβ accumulation

SDS-soluble $A\beta_{40}$ peptide quantitation was performed by ELISA as previously described.[15] Oxidative stress was estimated by immunohistochemistry using a monoclonal antibody against 8-hydroxy-2′-deoxyguanosine (8-OHdG) (a marker of nuclear and mitochondrial DNA oxidation). The methods are described online in the Supplementary Information.

### Laser cell microdissection and Quantitative PCR (qPCR) to evaluate mitochondrial content and mitochondrial DNA common deletion in hippocampal neurons

Rats were decapitated and brains were quickly removed and flash-frozen in isopentane. The tissue blocks were then cut into 20 μm sections, fixed in xylol and sandwiched between the metal-framed polyethylene naphthalate (PEN) membrane slides (Applied Biosystems, Life Technologies, Naerum, Denmark) and a supporting glass slide, and placed in the ArcturusXT™ LCM System instrument (Applied Biosystem, USA) equipped with an infrared (IR) capture laser (150 mW, maximum output at 804–813 nm) and a UV cutting laser (1W, 250 μJ, 15 ns pulse, maximum output at 349 nm) for LCM. Then, after the subiculum, CA1 and CA2 hippocampal neurons were identified, the thermoplastic ethylene vinyl acetate (EVA) membrane of the cap was melted and glued with the PEN membrane specifically over the area of interest by applying IR laser pulses. The targeted samples were released from the remainder of the tissue and the PEN membrane by cutting with the UV laser. The caps were then lifted, and following microscopic verification for the efficiency of the procedure, the captured cells were processed for the RNA or DNA extractions. Three cryosections were dissected from each rat brain and recovered in a single cap. DNA was isolated with Arcturus® PicoPure® DNA extraction kit following the manufacturer's instructions. The amount of mitochondria and the presence of *mt*DNA deletion were quantified by qPCR with gene-specific primers shown in the Supplementary Information (Table S1). *ND1* is a mitochondrial gene located out of the common deletion region (~4977 bp) and it is used to target total *mt*DNA; *ND4* is a mitochondrial gene located in the region of the common deletion and ~~CFTR~~ is a nuclear gene used as an indicator of genomic DNA. The ratios *ND1*/*CFTR* and *ND4*/*ND1* are indicative of the amount of mitochondria and *mt*DNA deletions, respectively. One to 50 μg of DNA recovered from cells isolated by LCM was used per well. Samples were plated in triplicate. SYBR-Green qPCR was performed by using the KAPA SYBR® FAST Universal 2X qPCR Master Mix (Kapa Biosystems). Reactions were run in an Mx3005P cycler (Stratagene) and results analyzed by the MxPro software in a Comparative Quantitation mode.

### Evaluation of energy metabolism and Aβ catabolism genes expression in hippocampi of 6-month-old Tg(+/−) rats

Two alternative procedures for RNA isolation were performed. RNA from iAβ containing neurons obtained by LCM was isolated with PicoPure RNA Isolation Kit (Applied Biosystems) and from hippocampal homogenates, a standard protocol was used.[7] RNA quality control and quantification were performed with a bioanalyzer (Agilent 2100). Samples with a RIN (RNA Integrity Number) value lower than 6 were discarded as indicative of degraded RNA. One microgram of total RNA was reverse transcribed using oligo(dT) primer and SuperScript II reverse

transcriptase (Invitrogen). *PGC-1a, NRF-1*, and *IDE-Met1* were targeted to assess the status of the energetic metabolism (*PGC-1a, NRF-1*) and Aβ catabolism (*IDE-Met1*) genes. Gene-specific primers are shown in Supplementary Information (Table S1). cDNA was amplified by SYBR Green RT-qPCR with a Mx3005P cycler (Stratagene). Cycling conditions were as follows: 95°C for 10 min, 95°C for 30 s, annealing for 30 s at 58°C, and 72°C for 30 s for 40 cycles. Melt curve analysis and agarose gels verified the formation of a single desired PCR product. The relative amount of transcripts to TATA-binding protein (*TBP*) was quantified by the $2^{-\Delta\Delta Ct}$ method using MxPro software.

### Statistical analysis

All data are shown as the mean ± SEM of at least three independent experiments. Data were analyzed by unpaired two-tailed Student's t-test, one and two-way ANOVA, or by two-way mixed ANOVA tests followed by Tukey's HSD post hoc tests for multiple comparisons, unless noted otherwise. The significance level was set at $p = 0.05$. SPSS 15.0 for Windows software (Chicago, IL, USA) was used to perform all statistical analyses.

## Results

### Hippocampal mitochondria of Tg(+/−) rats have lower complex I-dependent respiration, produce more $H_2O_2$, and accumulate more TBARS than WT rats

At a neuropathological level, Tg(+/−) rats are characterized by a subtle phenotype with an "age-independent" accumulation of iAβ in the hippocampus.[14,15] Mitochondria used for metabolic assays were isolated from hippocampus and the quality control of the preparation is shown in Supplementary Information (Figure S1). The effect of the human transgene on metabolic and oxidative parameters in isolated mitochondria of 6-month-old Tg(+/−) rats showed a significant decrease in state 4 and state 3 respiration in the presence of complex I substrates (malate and glutamate) as compared to WT rats (Table 1A1). By contrast, no significant differences were detected when the complex II substrate (succinate) was added (Table 1A2). In addition, ATP synthesis rate in the presence of glutamate and malate was significantly lower in Tg(+/−) as compared to WT rats (Table 1B) and significantly enhanced mitochondrial $H_2O_2$ generation (Table 1C) and TBARS accumulation (Table 1D) were detected at 6-month-old Tg(+/−) rats as compared to WT. However, Tg(+/−) sections positive for iAβ staining (Supplementary Information Figure S2, upper right panel) showed a negative reaction when probed with anti-8-OHdG, suggesting that these animals lack oxidation of nucleic acids. It is of note that the same antibody showed a positive labeling in brain sections of aged Tg2576 mouse, a "late stage" AD animal model characterized by extracellular deposition of Aβ (Supplementary Information Figure S2, lower right panel). To check whether the impairment in hippocampal mitochondrial function of 6-month-old Tg(+/−) rats was due to a reduced number of mitochondria and/or to the presence of the common deletion of *mt*DNA, we performed qPCR in iAβ positive neurons isolated by LCM. WT and Tg(+/−) animals showed a similar number of mitochondria although there was a

**Table 1.** Metabolic and oxidative parameters in isolated hippocampal mitochondria of 6-month-old rats.

| | Control (WT) | Transgenic Tg(+/−) |
|---|---|---|
| A. Oxygen consumption rate | | |
| 1. Malate + glutamate | | |
| State 4 (ng-at O/min/mg protein) | 26 ± 1 | 22 ± 1* |
| State 3 (ng-at O/min/mg protein) | 64 ± 1 | 51 ± 3* |
| 2. Succinate | | |
| State 4 (ng-at O/min/mg protein) | 17 ± 1 | 17 ± 1 |
| State 3 (ng-at O/min/mg protein) | 45 ± 2 | 38 ± 2 |
| B. ATP synthesis rate with Malate + glutamate as substrates (nmol/min/mg protein) | 122 ± 1 | 69 ± 4* |
| P/O ratio | 1.8 ± 0.1 | 1.3 ± 0.1** |
| C. $H_2O_2$ production rate with Malate + glutamate as substrates (nmol/min/mg protein) | 1.1 ± 0.1 | 1.4 ± 0.1* |
| D. TBARS (nmol/mg protein) | 2.1 ± 0.1 | 3 ± 0.1** |

Note: Data are expressed as the mean ± SEM of 6-month-old WT ($n = 5$) and Tg(+/−) ($n = 5$). State 4, resting respiration; State 3, active respiration. *$p < 0.05$; **$p < 0.01$ as compared to aged-matched WT.

trend to lower values (fold-change $-1.3 \pm 0.1$) in Tg(+/−) as compared to WT samples. The presence of the common deletion in *mt*DNA was ruled out in these cells since the mean values of *ND4*/*ND1* ratio in Tg(+/−) ($1.03 \pm 0.02$) were similar to WT (*ND4*/*ND1* = 1) (Supplementary Information Figure S3).

## *Hippocampal synaptosomes from Tg(+/−) rats have dysfunctional mitochondria*

To fully evaluate mitochondrial function in synaptosomes isolated from hippocampi of 6-month-old rats, we used an extracellular flux analyzer. The enrichment in synaptophysin (Figure 1(a), upper panel) and the morphology and size of particles obtained after the biochemical fractionation (Figure 1(a), lower panel) were used as criteria of quality control of the preparation of synaptosomes. As previously reported for guinea-pig and mouse synaptosomes, rat synaptosomes utilize exogenous glucose and pyruvate as substrates for active respiration.[22,23] Oxygen consumption rate (OCR) and extracellular acidification rate (ECAR) profiles of 6-month-old WT rat synaptosomes incubated with 15 mM glucose or 15 mM glucose plus 10 mM

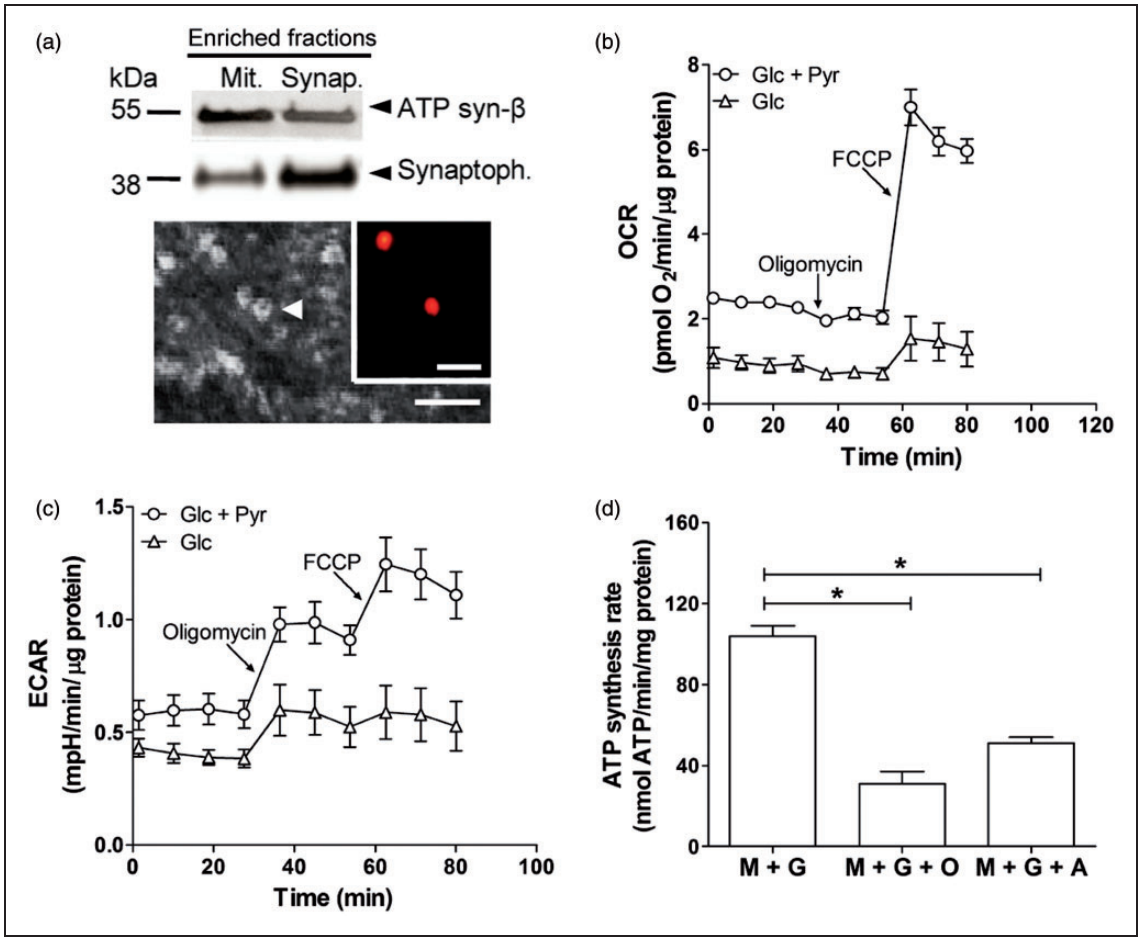


**Figure 1.** Biochemical and metabolic characterization of synaptosomes in 6-month-old WT rats. (a) Representative Western blotting of mitochondrial (Mit.) and synaptosomal (Synap.) enriched fractions immunoreacted with the mitochondrial ATP-synthase β subunit (ATP syn-β) and synaptosomal synaptophysin (Synaptoph.) protein markers antibodies (upper panel); frozen-thawed plate-attached synaptosomes were imaged using an Olympus CKX41 microscope (lower panel). Synaptosome with the characteristic 'doughnut' shape is indicated by arrowhead. Inset, typical autofluoresence of synaptosomes aggregates imaged using an Olympus BX50 microscope. Scale bars, 10 μm; inset, 50 μm. (b), Representative profile of the oxygen consumption rate (OCR) for hippocampal synaptosomes from 6-month-old WT rats. OCR was determined in the presence of 15 mM glucose or 15 mM glucose plus 10 mM pyruvate as substrates. Graph shows basal OCR, OCR after ATP synthase inhibition by 5 μM oligomycin and maximum OCR after the addition of 1 μM FCCP. Data are means ± SEM. (c) Graph shows the extracellular acidification rate (ECAR) determined in parallel with respiration shown in (b). (d) Bars show ATP synthesis rate in synaptosomes of 6-month-old WT rats assessed with luciferin-luciferase assay in digitonin-permeabilized samples in the presence of malate and glutamate (M + G) and after the addition of 1 μM oligomycin (O) or 5 μM antimycin (a). *$p < 0.05$ vs. M+G.

pyruvate were determined. Under these conditions, typical OCR and ECAR patterns were obtained measuring basal values and after the addition of oligomycin, FCCP and antimycin. Basal OCR (Figure 1b) is significantly increased in the presence of pyruvate, yet oxygen consumption with only glucose as substrate evidences the existence of glycolytic enzymes in synaptosomes. Coupling efficiency estimated after the addition of oligomycin in glucose/pyruvate medium (~13%) was improved (~30%) using glucose medium, reinforcing the concept that pyruvate translocation across mitochondrial membrane is proton coupled.[24] The addition of FCCP to WT synaptosomes uncoupled oxygen consumption from ATP synthesis, allowing determination of the maximum respiration and spare respiratory capacity. As expected, the presence of pyruvate highly increased the maximum respiration rate, and the spare respiratory capacity was ~3-fold higher than the basal respiration, suggesting that synaptosomal mitochondria can respond to an increase in energy demand. Moreover, the extracellular acidification rate (ECAR) in glucose/pyruvate medium increased after the addition of oligomycin and FCCP (Figure 1c), in agreement with the activation of anaerobic glycolysis in response to the inhibition of mitochondrial ATP synthesis.[21,22] In addition, we determined ATP synthesis rate in permeabilized WT synaptosomes in the presence of complex I substrates, malate and glutamate, before and after the addition of oligomycin or antimycin, respectively. Significant decrements were detected in ATP synthesis rate with oligomycin or antimycin (Figure 1d), suggesting that respiration in our synaptosomal preparation is coupled to ATP synthesis.

Since Aβ is known to localize to mitochondrial membranes, disrupt the electron transport chain, increase reactive oxygen species production, and cause mitochondrial damage,[25] we evaluated if these events could be responsible for mitochondrial dysfunction in our setting. In accordance with our previous observation in whole hippocampal homogenates,[15] we detected in synaptosomes of 6-month-old Tg(+/−) rats the presence of SDS-resistant Aβ oligomers (Figure 2a). Then, we compared the metabolic response of synaptosomes from Tg(+/−) and WT rats and showed that when maximal OCR was expressed as a fraction of WT basal value,[26] differences between WT and Tg(+/−) rats reached significance ($271 \pm 16$ % vs. $190 \pm 24$ %; $p < 0.05$) (Figure 2b) concordant with the respiratory deficits detected in isolated hippocampal mitochondria. Additionally, decrements in the respiratory control rate (RCR) ($2.6 \pm 0.4$ pmol$O_2$/min/μg protein vs $3.1 \pm 0.2$ pmol$O_2$/min/μg protein; $p = 0.05$) and in the spare respiratory capacity ($2.6 \pm 0.8$ pmol$O_2$/min/μg protein ~~vs~~ $4 \pm 0.3$ pmol$O_2$/min/μg protein; $p < 0.05$) were detected in synaptosomes from Tg(+/−) as compared to WT. Furthermore, the similar ECAR profile of WT and Tg(+/−) rats in basal conditions ($0.6 \pm 0.1$ mpH/min/μg protein and $0.5 \pm 0.2$ mpH/min/μg protein, respectively) showed no significant differences after the addition of oligomycin ($1 \pm 0.1$ mpH/min/μg protein vs $1 \pm 0.2$ mpH/min/μg protein; $p > 0.05$) or FCCP ($1.2 \pm 0.1$ mpH/min/μg protein vs $1.1 \pm 0.3$ mpH/min/μg protein; $p > 0.05$).

## *Synaptosomes of Tg(+/−) rats show decreased complex I enzymatic activity as compared to WT*

We wondered whether the decrease in spare respiratory capacity and mitochondrial respiratory control ratio may be the consequence of impaired neuronal anterograde transport of mitochondria from the soma to the synapses. Thus, we determined by two different experimental approaches the number of mitochondria in synaptosomes of 6-month-old Tg(+/−) and WT rats. No significant differences were detected between WT and Tg(+/−) animals in the amount of mitochondrial protein (ATP synthase β subunit) as determined by Western blotting (Figure 2c) and expressed as arbitrary units (A.U.) ($0.49 \pm 0.1$ vs. $0.5 \pm 0.1$), nor in the activity of citrate synthase enzyme (a stable mitochondrial matrix protein) (Figure 2d) ($336.4 \pm 16.5$ vs. $312.5 \pm 32.1$ nmol/min/mg protein). To further analyze the respiratory chain mitochondrial complexes and the tricarboxylic acid (TCA) cycle functionality, we evaluated complex I, complex II and α-KGDHC activities at the synapses of WT and Tg(+/−) rats of 6 months of age. Our results showed (Figure 2e) significant decrements in complex I ($338 \pm 13$ nmol/min/mg ~~vs~~ $216 \pm 29$ nmol/min/mg; $p < 0.05$) but not in complex II ($16 \pm 5$ nmol/min/mg ~~vs~~ $7 \pm 2$ nmol/min/mg; $p = 0.1$) nor in α-KGDHC ($19 \pm 2$ nmol/min/mg vs. $23 \pm 1$ nmol/min/mg; $p = 0.09$) enzymatic activities suggesting that bioenergetic impairments at the synapses may be due to a direct impact of *mit*Aβ on complex I but not on α-KGDHC as shown in AD brains.[27,28] To assess whether in Tg(+/−) rat brains there is a dysregulation of PGC-1α/NRF-1/IDE-Met1 pathways mediated by Aβ accumulation as reported in the AD brain and *in vitro*,[7] we determined the levels of these transcripts in iAβ positive cells isolated by LCM. Since the quality control of RNA (RIN<6) precluded its utilization for qRT-PCR and to partially answer this question, we used RNA isolated from hippocampal homogenates. In contrast to NRF-1 and IDE-Met1 genes that did not show variation, in 6-month-old Tg(+/−) rats transcript levels of PGC-1α gene decreased 1.9-fold, as compared to aged-matched controls (WT=1) (Figure 2f), suggesting that in Tg(+/−) rats the PGC-1α pathway is altered. In addition, we evaluated

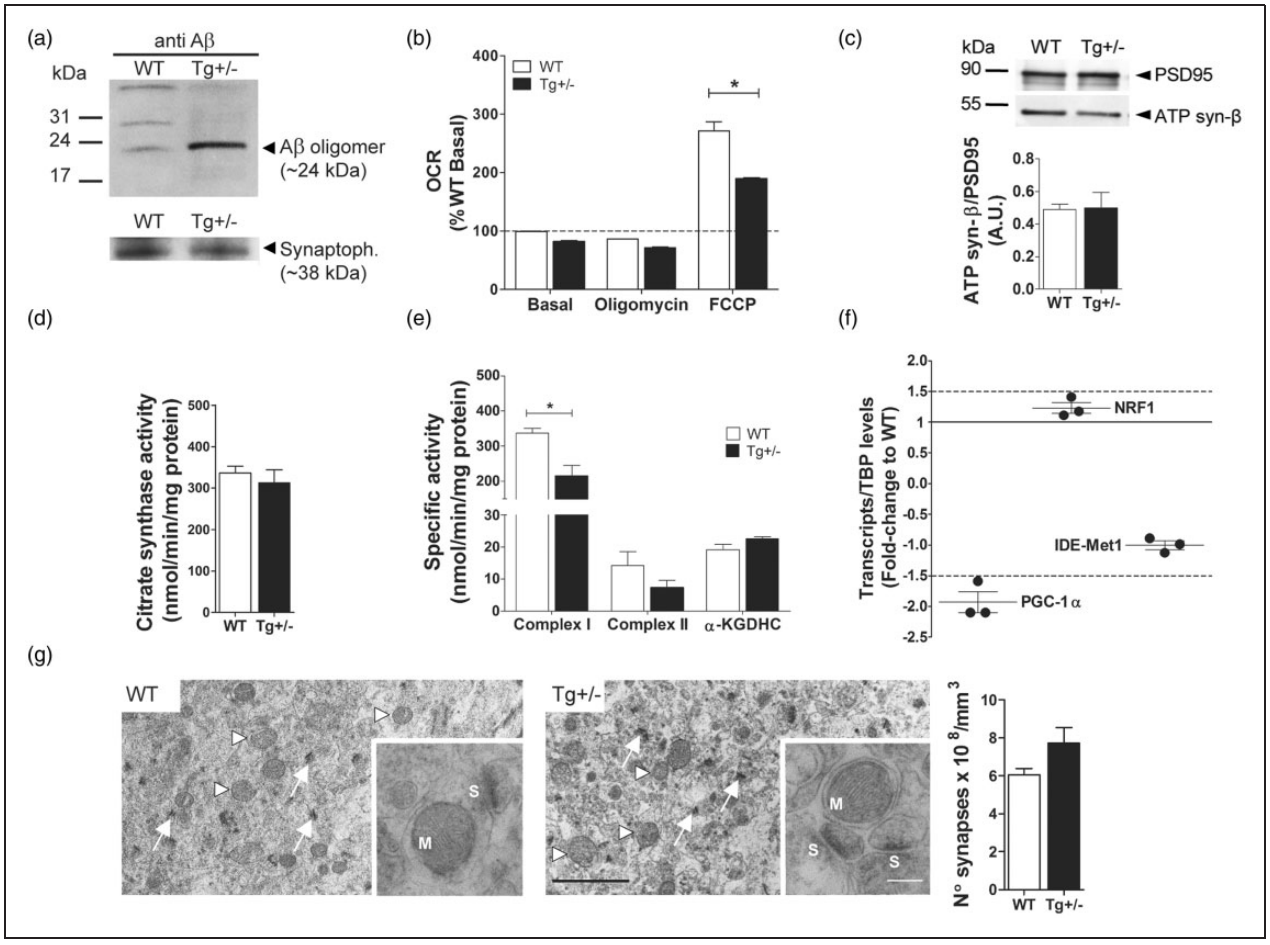


**Figure 2.** Mitochondrial function of hippocampal synaptosomes from 6-month-old Tg(+/−) rats. (a) Representative Western blotting (upper panel) of pools corresponding to WT and Tg(+/−) synaptosomes showing Aβ oligomers (≈ 24 kDa) in Tg(+/−) in contrast to WT samples. Protein content of each lane is shown by anti-synaptophysin immunoreactivity (≈ 38 kDa) (lower panel). (b) Bars show the oxygen consumption rate (OCR) of synaptosomes of WT and Tg(+/−) rats expressed as % of WT basal value. *$p < 0.05$ vs. WT. (c) Representative Western blotting of synaptosomes of WT and Tg(+/−) rats immunoreacted with the synaptosomal (PSD-95) and mitochondrial ATP-synthase β-subunit (ATP syn-β) protein markers (upper panel). Bars (lower panel) show the semi-quantification of 6–7 biological replicates of mitochondrial proteins normalized by synaptosomal content expressed in arbitrary units (A.U.) Data are means ± SEM. $p = 0.9$. (d) Bars show the citrate synthase activity of WT and Tg(+/−) synaptosomes expressed as nmol/min/mg protein. Data are means ± SEM. $p = 0.6$. (e) Bars show the specific activity of respiratory complex I, complex II and α-KGDHC of WT and Tg(+/−) synaptosomes expressed as nmol/min/mg protein. Data are means ± SEM. *$p < 0.05$ vs. WT. (f) The endogenous PGC-1α, NRF-1, and IDE-Met1 transcript levels were determined by RT-qPCR from hippocampal homogenates of WT and Tg(+/−) rats. Each point represents the mean value of at least three independent experiments performed by triplicate for each sample normalized by TATA-binding protein (TBP). The mean ± SEM in Tg(+/−) relative to WT are shown. Values between dashed lines (+1.5 and −1.5) were considered not different from WT=1. (g) Electron micrograph of a portion of the CA1 hippocampal region from WT and Tg(+/−) rats. Arrows, synapses; arrowheads, mitochondria. Scale bar = 2 μm. Inset, high magnification showing a representative mitochondria (M) and synapse (S). Scale bar = 500 nm. Bars (left panel) show the number of synapses/volume. Data are means ± SEM. $p = 0.07$.

by transmission electron microscopy whether there were any synaptic changes at the CA1 region in Tg(+/−) as compared to WT rats. Stereological analysis of the images (Figure 2(g), left and middle panels) showed that the number of synapses/mm$^3$ (Figure 2(g), right panel) and the morphology of mitochondria were similar between Tg(+/−) and WT rats (diameter: 0.4 ± 0.1 μm vs. 0.4 ± 0.1 μm; axial ratio: 1 ± 0.1 μm vs. 1 ± 0.2 μm; circularity ratio: 1.4 ± 0.4 μm vs. 1.3 ± 0.3 μm; p = n.s. for all cases). Western blotting of PSD-95, a marker of synaptic integrity[29,30] did not show significant differences between Tg(+/−) and WT rats (Figure S4, Supplementary Information). Together, these results suggest that the metabolic changes in Tg(+/−) synaptosomes were not due to a reduced number of mitochondria or synaptic loss.

### *PQQ prevented cognitive impairment and synaptic mitochondrial dysfunction of Tg(+/−) rats*

To assess the effect of BioPQQ upon behavioral, cognitive and biochemical variables, 6-month-old rats belonging to three groups (WT; Tg(+/−) and Tg(+/−)+BioPQQ) were evaluated. Gross inspection of each rat prior to the behavioral experiments did not reveal any visible differences between WT and Tg(+/−) animals. All animals appeared healthy and neurological reflexes were normal. The three groups exhibited similar levels of spontaneous locomotor activity and rear frequency in the elevated plus maze (EPM) and open field (OF) tests (Table 2). Moreover, no differences were detected in anxiety-related behaviors among groups in the EPM (Table 2). By contrast, Tg(+/−) displayed a more anxious phenotype than WT rats as they showed a lower number of entries and spent less time in the center of the OF (two-tailed Mann-Whitney $U = 11$, $p < 0.05$; $U = 9$, $p < 0.05$, respectively) (Figure 3a) as previously reported.[15] The treatment with BioPQQ did not modulate the anxious behaviors in the OF, since Tg(+/−)+BioPQQ group did not behave differently than the other two groups (Figure 3a). Spontaneous locomotor activity in the Y-maze was similar (Figure 3(b), left axis) while the percentage of alternations (Figure 3(b), right axis) was significantly different (one-way ANOVA, $F_{(2, 24)} = 7$, $p < 0.01$) among groups. Tg(+/−) rats exhibited a significant lower percentage of alternation in comparison to WT and Tg(+/−)+BioPQQ rats ($p < 0.01$; $p < 0.05$, respectively) which is indicative of an spatial working memory impairment. These results replicate previous findings by our group.[15] The treatment with BioPQQ prevented this memory impairment, since the Tg(+/−)+BioPQQ group showed a percentage of alternations similar to WT (Figure 3(b), right axis). Paired *t*-tests indicated that during the sample trial of the Novel Object Recognition Task (NORT), the three groups of animals explored a similar amount of time the two identical sample objects (WT: $t = 0.3$, p = n.s.; Tg(+/−): $t = 1.1$, p = n.s.; Tg(+/−)+BioPQQ: $t = 0.6$, p = n.s.) (Figure 3(c)). During the retention trial, all groups were able to discriminate the novel from the familiar object, exploring significantly more time the former than the latter (paired *t*-tests. WT: $t = 3.2$, $p < 0.01$; Tg(+/−): $t = 2.9$, $p < 0.01$; Tg(+/−)+BioPQQ: $t = 2.4$, $p < 0.05$) (Figure 3d). These results suggest that recognition memory was unaltered. Spatial learning and reference memory was evaluated with the Morris water maze (MWM) test. All groups significantly reduced their latencies and path lengths (Figure 4(a), upper left panel and upper right panel, respectively) during the second day of cued learning in the MWM (*Latency*. Day: $F_{(1, 24)} = 258.5$, $p < 0.01$; Group: $F_{(2, 24)} = 1.4$, p = n.s.; Day × Group: $F_{(2, 24)} < 1$, p = n.s. *Path length*. Day: $F_{(1, 24)} = 160.2$, $p < 0.01$; Group: $F_{(2, 24)} < 1$, p = n.s.; Day × Group: $F_{(2, 24)} < 1$, p = n.s.) and no significant differences in swim speed were detected (Figure S5, left panel). These results suggest that groups were not visually impaired and had no deficits in swimming abilities. Regarding the spatial learning all groups were able to learn the task at an equivalent rate (Figure 4(a), lower left panel and lower right panel) (*Latency*. Day: $F_{(4, 96)} = 42.3$, $p < 0.01$; Group: $F_{(2, 24)} < 1$, p = n.s.; Day × Group: $F_{(8, 96)} < 1$, $p$ = n.s. *Path length*. Day: $F_{(4, 96)} = 45$, $p < 0.01$; Group: $F_{(2, 24)} < 1$, p = n.s.; Day × Group: $F_{(8, 96)} < 1$, p = n.s.) and swim speed was similar among groups across the 5 days of training (Figure S5, right panel). Twenty-four hours after the last spatial learning trial, the escape platform was removed from the tank and the probe trial was conducted. By contrast to Tg(+/−) group, the WT and Tg(+/−)+BioPQQ groups showed higher percentages of time spent in the target quadrant than expected by chance (Figure 4b) (two-tailed paired Wilcoxon signed-rank test, $Z = -2.2$, $N = 7$, $p < 0.01$ (WT); $Z = -2.4$, $N = 8$, $p = 0.01$ (Tg(+/−) + BioPQQ); $Z = -0.3$, $N = 5$, p = n.s. (Tg(+/−)). Furthermore, WT

**Table 2.** Assessment of spontaneous locomotion and anxiety-related behaviors.

| | WT | Tg(+/−) | Tg(+/−)+PQQ | One-way ANOVA |
|---|---|---|---|---|
| EPM | | | | |
| Distance covered (cm) | 967.9 ± 77.2 | 938.7 ± 109.2 | 946.5 ± 124.7 | $F_{(2, 24)} = 0.19$, $p$ = n.s. |
| Number of closed arm entries | 9.0 ± 0.9 | 8.7 ± 0.8 | 9.1 ± 0.7 | $F_{(2, 24)} = 0.07$, $p$ = n.s. |
| Open arm entries (%) | 14.8 ± 5.3 | 9.2 ± 4.1 | 11.9 ± 4.7 | $F_{(2, 24)} = 0.35$, $p$ = n.s. |
| Time in open arms (%) | 7.1 ± 3.0 | 4.3 ± 2.0 | 5.2 ± 1.9 | $F_{(2, 24)} = 0.37$, $p$ = n.s. |
| OF | | | | |
| Distance covered (cm) | 1384.4 ± 73.6 | 1225.2 ± 95.7 | 1317.5 ± 196.4 | $F_{(2, 24)} = 0.35$, $p$ = n.s. |
| Number of rears | 17.0 ± 1.36 | 15.9 ± 1.6 | 15.2 ± 1.9 | $F_{(2, 24)} = 0.26$, $p$ = n.s. |

Note: Data are expressed as the mean ± SEM of WT ($n = 8$), Tg(+/−) ($n = 10$) and Tg(+/−)+PQQ ($n = 9$) animals. EPM, elevated plus maze; OF, open field.

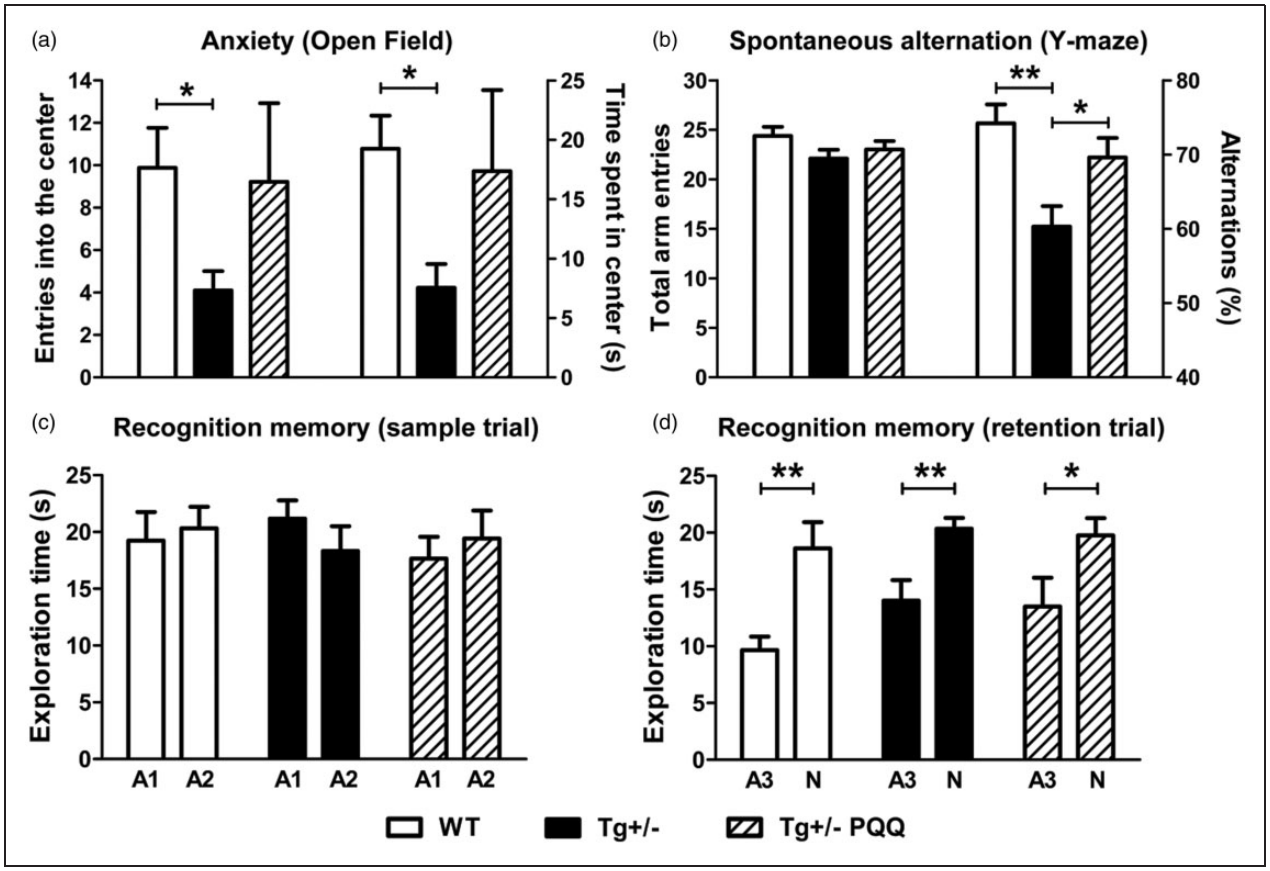


**Figure 3.** Effect of BioPQQ on anxiety, spatial working memory and recognition memory. Bars show in (a), entries into the center (left axis) and time spent in the center (right axis) of the OF; (b) total arm entries (left axis) and percentage of alternation (right axis) in the Y-maze; (c) exploration times for the two identical objects (A1 and A2) during the sample trial in the NORT; (d) exploration times for the familiar (A3, identical to A1 and A2) and novel (N) object. Data are means ± SEM of 8–10 rats per group. $^{*}p < 0.05$, $^{**}p < 0.01$.

and Tg(+/−)+BioPQQ groups exhibited a significantly higher percentage of time in the target quadrant than Tg(+/−) group (Figure 4b) (two-way mixed ANOVA, Quadrant: $F_{(3,\ 72)} = 6.45$, $p < 0.01$; Group: $F_{(2,\ 24)} < 1$,, p = n.s.; Quadrant × Group: $F_{(6,\ 72)} = 1.9$, p = n.s. followed by Tukey's post-hoc tests, $p < 0.01$ and $p < 0.05$, respectively). In addition, WT and Tg(+/−)+BioPQQ groups showed similar periods of time spent in the target quadrant (Figure 4b). These results indicate that Tg(+/−) rats exhibited an impaired spatial reference memory, as previously reported,[15] and that the treatment with BioPQQ was able to prevent it.

To assess whether the cognitive improvement was related to a better metabolic response at the synapses, we determined the spare respiratory capacity of synaptosomes. When we expressed the spare respiratory capacity as a fraction of WT, differences between Tg(+/−) and Tg(+/−)+BioPQQ rats reached significance (69 ± 7% vs. 97 ± 3%; $p < 0.05$) (Figure 5a). This result suggests that cognitive improvements due to BioPQQ may be related to a better synaptic mitochondrial functionality. The improving effect of BioPQQ was not mediated by promotion of mitochondrial biogenesis or reduction of iAβ levels, since no significant differences were observed in the number of mitochondria as determined by qPCR from DNA of iAβ positive cells isolated by LCM from Tg(+/−) and Tg(+/−)+BioPQQ (Figure 5b) or in the levels of SDS-soluble Aβ determined by ELISA in hippocampal homogenates of Tg(+/−) and Tg(+/−)+BioPQQ rats (9.2 ± 1.7 pg Aβ/mg vs. 8.2 ± 2.8 pg Aβ/mg; p=0.75). Moreover, at the synaptic level, no significant differences were observed in the amount of a mitochondrial protein (ATP synthase β subunit) determined by Western blotting (Figure 5c). Knowing that BioPQQ may exert an anti-oxidant effect,[31] we assessed TBARS in hippocampal mitochondria from Tg(+/−)+BioPQQ animals. Our results showed that BioPQQ treatment reversed the oxidative damage to phospholipids (Figure 5d) (3.4 ± 0.4 nmol/mg protein vs 2 ± 0.1 nmol TBARS/mg protein; $p < 0.05$).

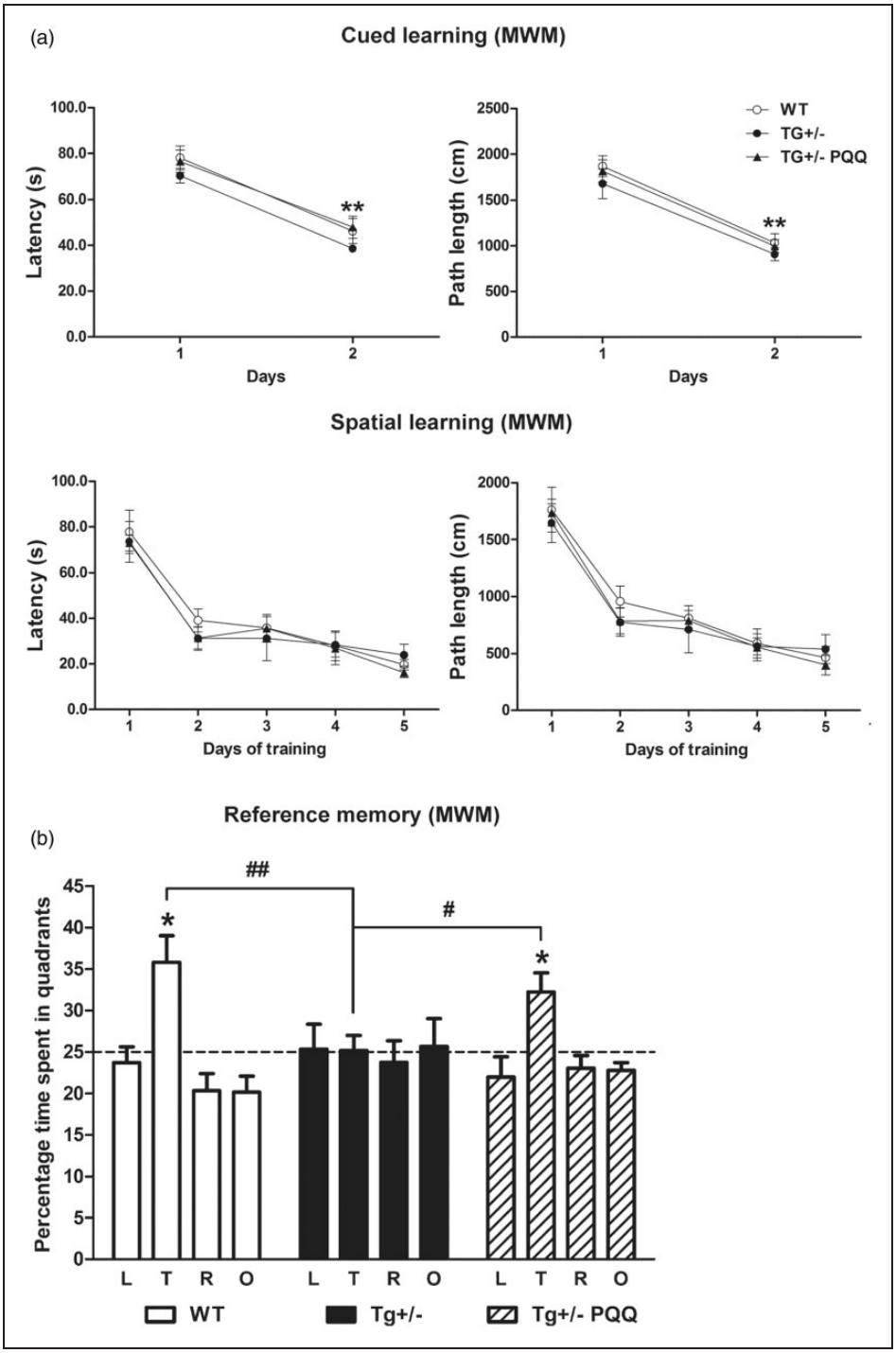


**Figure 4.** Treatment with BioPQQ prevented the spatial reference memory deficit exhibited by Tg(+/−) rats. (a) Graphs show latencies (upper-left panel) and paths length (upper-right panel) during the first and second day of the cued learning and latencies (lower-left panel) and paths length (lower-right panel) throughout the five days of spatial learning in the MWM test. (b) Bars show the percentage of time spent in quadrants (L, left; T, target; R, right; O, opposite). Data are means ± SEM of 8–10 per group. $^{*}p < 0.05$ vs. percentage of time expected by chance (dashed line), $^{\#}p < 0.05$, $^{\#\#}p < 0.01$.

## Discussion

The primary objective of the present study was to analyze early synaptic bioenergetics compromise in the progression of the AD-like amyloid pathology. To reach this goal, we resorted to use transgenic rats. Rats have advantage over mice because they are phylogenetically closer to humans, have postnatal CNS

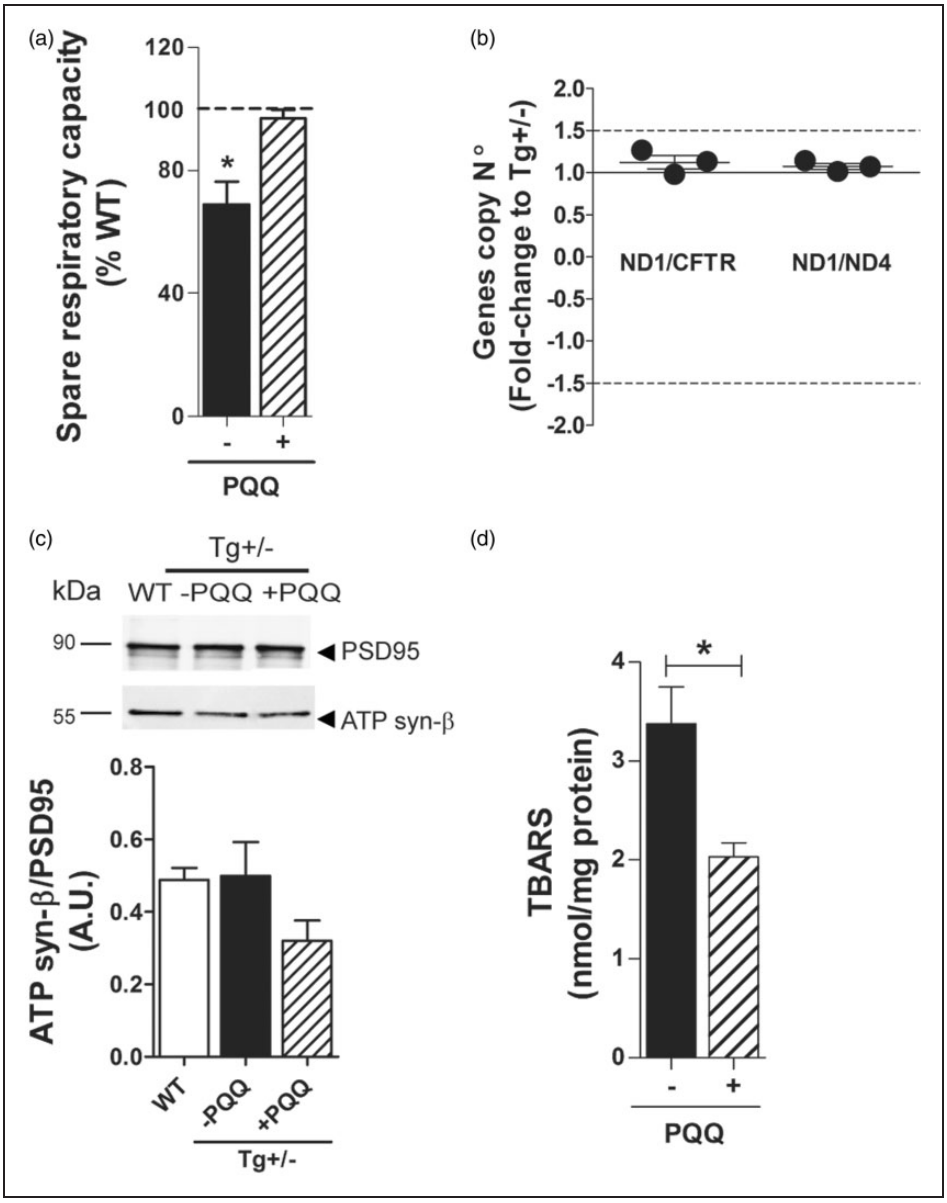


**Figure 5.** Biochemical impact of BioPQQ on synaptic mitochondrial functionality and brain oxidative stress in 6-month-old Tg(+/−) rats. (a) Bars show the spare respiratory capacity of synaptosomes from Tg(+/−) rats under control (black) or BioPQQ (dashed) supplemented diet expressed as % of WT. *$p < 0.05$ vs. Tg(+/−) + BioPQQ; (b) The gene copy number of endogenous *ND1* was determined by qPCR from CA1 iAβ positive neurons microdissected by LCM from Tg(+/−) and Tg(+/−)+BioPQQ rats. Each point represents the mean value of at least three independent experiments performed by triplicate for each sample normalized by cystic fibrosis transmembrane conductance regulator (*CFTR*) (left) and *ND4* (right) gene, respectively. The mean ± SEM in Tg(+/−)+BioPQQ relative to Tg(+/−) is shown. Values between dashed lines (1.5 and −1.5) were considered not different from Tg(+/−)=1. (c) Representative Western blotting of synaptosomes of WT, Tg(+/−) and Tg(+/−)+BioPQQ rats immunoreacted with the synaptosomal (PSD-95) and mitochondrial ATP-synthase β-subunit (ATP syn-β) protein markers (upper panel). Bars show the semi-quantification of 6–7 biological replicates of mitochondrial protein ATP syn-β normalized by PSD-95 content expressed in arbitrary units (A.U.). $F_{(2,13)}$, $p = 0.35$. (d) Bars show TBARS accumulation expressed as nmol/mg protein in hippocampal mitochondria of Tg(+/−) rats exposed to control (black) or BioPQQ (dashed) diet. Data are means ± SEM. *$p < 0.05$.

development, and show a more complex brain connectome and a richer behavioral display.[32] Different transgenic rat models of AD were developed in the last 10 years.[33] Among these, the McGill-R-Thy1-APP transgenic rat is of particular interest because AD-like pathology is achieved with a single transgene (human APP with 2 familial Alzheimer's disease mutations) and a single insertion site per allele making of it an AD

transgenic model with a low transgene dosage. We opted to use hemizygous (+/−) adult animals (6-month-old) because they display iAβ accumulation and cognitive deficits similar to early AD. First, we showed that there are a number of significant biochemical abnormalities in mitochondria derived from bulk preparations of hippocampal tissue in Tg(+/−) rats. An effect of the expression of the human APP751 transgene with the Swedish and Indiana mutation and/or its proteolytic products including Aβ, on oxygen consumption is clearly observed in Tg(+/−) animals. Inhibition of active (state 3) and resting (state 4) respiration was detected in 6-month-old Tg(+/−) rats as compared to WT. These effects were evident when complex I substrates were used and may be indicative of complex I decreased activity, as described in AD brains.[34] Moreover, a significant decrement in mitochondrial ATP production rate was observed in Tg(+/−) hippocampi, suggesting the existence of a profound bioenergetic impairment in the brain of these animals. Different molecular mechanisms have been proposed for complex I inactivation including the synergistic inhibition produced by peroxynitrite-mediated reactions, reactions with free radical intermediates of lipid peroxidation and amine–aldehyde adduction reactions. More recently, alterations in complex I assembly intermediates precluding the proper formation of supercomplexes or respirasomes has been proposed.[35] The decrease in the oxygen consumption rate detected in 6-month-old Tg(+/−) rats may be due to an alteration in the redox equilibrium in the hippocampus in these animals. Mitochondria from 6-month-old Tg(+/−) rats produced more hydrogen peroxide and increased the accumulation of lipid oxidation products (TBARS). These results indicate that under basal metabolic conditions, Tg(+/−) brain is undergoing a sustained mitochondrial oxidative damage which may be responsible of the respiratory impairments with age.

Our results provide strong evidence that in Tg(+/−) rats there is an increasing mitochondrial vulnerability associated to the expression of the human transgene. However, we showed that 8-OHdG positive cells, described in AD brains,[36] are absent in the hippocampus of 6-month-old Tg(+/−) rats, but present in aged Tg2576 mice. Differences observed in oxidation of *mt*DNA mediated by ROS[37] in both AD animal models may be due to different expression levels of the human transgene (Tg2576 mice express mutated human APP at 7-fold while Tg(+/−) rats at 2-fold over endogenous APP) and/or the brain Aβ burden (Tg(+/−) rats show intracellular accumulation while Tg2576 mice extracellular deposits).

Isolated mitochondria from hippocampal homogenates possess a number of disadvantages to identify neuronal specific deficits and organella functionality in the cytoplasmic environment. To overcome this situation, we performed synaptosomal assays, as the synaptosome is by definition derived from neurons. Although isolated synaptosomes were not 100% pure, fluorescence microscopy indicated that broken synaptosomes were undetectable. Our results showed that maximum respiration, obtained in the presence of an uncoupler, was lower in equivalent amounts of synaptosomes (with equivalent mitochondrial content) isolated from Tg(+/−) rats than in those isolated from WT. In a broader sense, we compared the spare respiratory capacity of the synaptosomes and demonstrated the existence of mitochondrial dysfunction under conditions of energetic load. Spare respiratory capacity reflects the ability of mitochondria to meet increased energy demand with increased respiration and it is considered as a primary factor to define survival of neurons under stress.[38] Synaptosomes from Tg(+/−) rats also presented a decrease in the respiratory control ratio, and this parameter (sensitive to substrate oxidation and proton leak) also supports the existence of mitochondrial dysfunction, and has the virtue of internal normalization.[21] In addition, the examination of the ECAR profile of synaptosomes showed that the nerve terminals from Tg(+/−) rats are unable to compensate for the loss of mitochondrial respiration with glycolytic activity. A shift towards glycolytic energy production was suggested to be a protective ''short-term'' mechanism in neuronal tissue that eventually leads to a ''long-term'' bioenergetic deficit and cell death.[39] In this sense, our results *ex vivo* are opposite to previous findings showing that an increased flux through glycolysis ''protects'' primary neuronal cultures from death induced by Aβ.[40] Respiratory properties of synaptosomes from commonly used Tg mouse models of late-AD have been reported and showed no consistent bioenergetic defects as compared to WT mice.[13] By contrast, here we show that, similar to what was detected at early stages in AD brain,[41] synaptosomes isolated from Tg(+/−) rats show respiratory dysfunction suggesting that, in this model, interaction of oligomeric Aβ with mitochondria at the synaptic level may be responsible of the bioenergetic failure. In addition, synaptosomes of Tg(+/−) showed reduced respiratory chain complex I catalytic activity but not complex II or α-KGDHC as compared to WT rats. Together this profile suggests in Tg(+/−) rats a pattern of differential sensitivity of mitochondrial enzymes to oxidative damage similar to what has been found in AD brains at early stages of the disease. It was previously reported that when one of the components of α-KGDHC was knocked-down in a Tg mouse model of amyloid deposition, increments in ROS and protein tyrosine nitration were observed.[42] Our results suggest that iAβ accumulation generates ROS by a mechanism different from α-KGDHC

inhibition. Experimental evidence suggest that PGC-1α is a powerful regulator of ROS removal by increasing the expression of numerous ROS-detoxifying enzymes with a critical impact in aging and AD.[43] In agreement with this concept, here we showed that in Tg(+/−) rats hippocampal level of PGC-1α is reduced, and the amount of $H_2O_2$ increased and mitochondrial metabolism impaired. Moreover, the identification that PGC-1α mRNA expression is reduced in Tg(+/−) brain as compared to WT, reinforces the concept that this pathway has a functional significance in mitochondrial activity and AD pathology. Synaptic loss correlates with cognitive impairment in demented patients.[44] However, we showed that the number of synapses per volume is not affected at CA1 in Tg(+/−) rats where iAβ accumulates. Since CA1 is a critical region of the cortico-hippocampal system for memory processing, our results suggest that functional rather than structural changes may account for the memory impairments in this animal model. It was recently reported that in a setting of energy failure due to mitochondrial dysfunction, neurons may attenuate neurotransmitters endocytosis to preserve ATP consumption.[45] In this regard, defects in vesicle recycling have been linked to short-term synaptic plasticity, memory, and cognitive impairment.[46] Alternatively, known mechanisms of Aβ toxicity include the disruption of intracellular $Ca^{2+}$ homeostasis and over stimulation of synaptic and extra-synaptic glutamatergic receptors[47] with potential impact in behavior without gross synaptic integrity alterations. Recently, a longitudinal testing of hippocampal plasticity in freely behaving McGill-R-Thy1-APP homozygous animals revealed an age-dependent and persistent inhibition of long-term potentiation without a change in baseline synaptic transmission in the CA1 area suggesting that synaptic long-term potentiation is selectively disrupted in these animals prior to extracellular deposition of Aβ.[48] These *in vivo* experiments are in agreement with our *in vitro* biochemical tests and corroborate the impact of the metabolic impairments in cognition and behavior. Brain hypometabolic state occurs in patients with mild cognitive impairment and was also observed in Tg mouse models of AD with cerebral amyloid angiopathy (arcAβ mice) prior to the detection of Aβ plaque pathology.[49] This evidence suggests that neurotoxic soluble Aβ species may disrupt brain blood flow compromising the supply of oxygen and essential metabolic precursors.[50] It is important to note that Tg(+/−) rats do not show cerebral amyloid angiopathy detectable by immunohistochemistry. Further analysis should be performed in isolated microvessels in order to evaluate the existence of vascular Aβ in these animals and its potential impact on hippocampal mitochondrial deficits.

At the level of the synaptosome, our results showed that the restricted electron transport capacity, possibly due to complex I inactivation, results in a slow progressive bioenergetic failure of a sub-population of vulnerable terminals when challenged with an increased energy demand. This phenotype could be, in part, responsible for the poor performance in the hippocampal dependent tasks.

Interestingly, the treatment with BioPQQ prevented the cognitive impairment as shown by the performance in the Y-maze and in the probe trial of the MWM test. Our results are in accordance with previous reports showing that PQQ treatment improves learning abilities in the MWM and prevents reference memory deficits when rats were subjected to hyperoxia.[31] Moreover, PQQ blocks spatial learning and memory deficits associated with aging[51] in rats. Furthermore, administration of PQQ in combination with a low dose of lithium restored the spatial learning and memory impairments in the APP/PS1 transgenic mouse model of AD.[52] In the present study, we showed that the treatment with BioPQQ partially restored the bioenergetic synaptic deficits in Tg(+/−) rats by mechanisms beyond mitochondrial biogenesis suggesting that other reported neuroprotective effects of BioPQQ such as its anti-oxidant effect,[31] its interaction with the NMDA receptor redox modulatory site,[53] and/or the stimulation of nerve growth factor production could underlie the prevention of bioenergetics and cognitive deficits.

In sum, to our knowledge this is the first report showing bioenergetics deficits in synaptosomes from a rodent model of AD and we propose that this rat model could provide insight into the bioenergetic changes which occur *in vivo* at early-stages of the disease, reinforcing the utility of this model as a platform for understanding the earlier biological basis of this progressive neurodegenerative disease and its pharmacologic manipulation.

## Funding

Grants from Consejo Nacional de Investigaciones Científicas y Técnicas (CONICET-PIP 378) (to LM), Alzheimer's Association (IIRG-11-205127) (to EMC), Agencia Nacional de Promoción Científica y Tecnológica (PICT 2013-318) (to EMC); Canadian Institute for Health and Research (MOP-97776) (to ACC), Comisión Sectorial de Investigación Científica (CSIC) (to CQ) and Agencia Nacional de Investigación e Innovación (ANII) (to CQ). PVMA and PG are supported by CONICET fellowships. SDC is holder of a Charles E Frosst-Merck post-doctoral fellowship. LM, EMC, and MCL are investigators of CONICET. ACC is holder of a

McGill University Charles E Frosst-Merck Chair in Pharmacology.

## Acknowledgements

We would like to thank Cecilia Rotondaro and Ágata Fernández Gamba from ~~Leloir Institute~~ for their helpful assistance in histologic and imaging process techniques and to Juan Félix López Téllez from Andalusian Centre for Nanomedicine and Biotechnology (BIONAND) for the electron microscopy analysis.

## Declaration of conflicting interests

The author(s) declared no potential conflicts of interest with respect to the research, authorship, and/or publication of this article.

## Authors' contribution

PVMA, NM and PG performed research; PVMA, CQ and LM designed research; PVMA, CQ, NM, PG, PE, AC, MCL, EMC and LM analyzed data; PG performed statistical analysis; CQ, PE, SDC and ACC contributed with unpublished reagents/analytic tools; PVMA, PG and LM wrote the paper.

## Supplementary material

Supplementary material for this paper can be found at http://jcbfm.sagepub.com/content/by/supplemental-data

## References

1. Hardy J and Allsop D. Amyloid deposition as the central event in the aetiology of Alzheimer's disease. *Trends Pharmacol Sci* 1991; 12(10): 383–388.
2. Adriaanse SM, Binnewijzend MA, Ossenkoppele R, et al. Widespread disruption of functional brain organization in early-onset Alzheimer's disease. *PLoS One* 2014; 9: e102995.
3. Rapoport SI, Hatanpaa K, Brady DR, et al. Brain energy metabolism, cognitive function and down-regulated oxidative phosphorylation in Alzheimer disease. *Neurodegeneration: A journal for neurodegenerative disorders, neuroprotection, and neuroregeneration* 1996; 5: 473–476.
4. Liang WS, Reiman EM, Valla J, et al. Alzheimer's disease is associated with reduced expression of energy metabolism genes in posterior cingulate neurons. *Proc Natl Acad Sci U S A* 2008; 105: 4441–4446.
5. Keil U, Bonert A, Marques CA, et al. Amyloid beta-induced changes in nitric oxide production and mitochondrial activity lead to apoptosis. *J Biol Chem* 2004; 279: 50310–50320.
6. Swerdlow RH and Khan SM. A ''mitochondrial cascade hypothesis'' for sporadic Alzheimer's disease. *Med Hypotheses* 2004; 63: 8–20.
7. Leal MC, Magnani N, Villordo S, et al. Transcriptional regulation of insulin-degrading enzyme modulates mitochondrial amyloid beta (Abeta) peptide catabolism and functionality. *J Biol Chem* 2013; 288: 12920–12931.
8. Killgore J, Smidt C, Duich L, et al. Nutritional importance of pyrroloquinoline quinone. *Science* 1989; 245: 850–852.
9. Smidt CR, Unkefer CJ, Houck DR, et al. Intestinal absorption and tissue distribution of [14C]pyrroloquinoline quinone in mice. *Proc Soc Exp Biol Med* 1991; 197: 27–31.
10. Jensen FE, Gardner GJ, Williams AP, et al. The putative essential nutrient pyrroloquinoline quinone is neuroprotective in a rodent model of hypoxic/ischemic brain injury. *Neuroscience* 1994; 62: 399–406.
11. Trushina E, Nemutlu E, Zhang S, et al. Defects in mitochondrial dynamics and metabolomic signatures of evolving energetic stress in mouse models of familial Alzheimer's disease. *PLoS One* 2012; 7: e32737.
12. Balietti M, Giorgetti B, Casoli T, et al. Early selective vulnerability of synapses and synaptic mitochondria in the hippocampal CA1 region of the Tg2576 mouse model of Alzheimer's disease. *J Alzheimers Dis* 2013; 34: 887–896.
13. Choi SW, Gerencser AA, Ng R, et al. No consistent bioenergetic defects in presynaptic nerve terminals isolated from mouse models of Alzheimer's disease. *J Neurosci* 2012; 32: 16775–16784.
14. Leon WC, Canneva F, Partridge V, et al. A novel transgenic rat model with a full Alzheimer's-like amyloid pathology displays pre-plaque intracellular amyloid-beta-associated cognitive impairment. *J Alzheimers Dis* 2010; 20: 113–126.
15. Galeano P, Martino Adami PV, Do Carmo S, et al. Longitudinal analysis of the behavioral phenotype in a novel transgenic rat model of early stages of Alzheimer's disease. *Front Behav Neurosci* 2014; 8: 321.
16. Bauerly K, Harris C, Chowanadisai W, et al. Altering pyrroloquinoline quinone nutritional status modulates mitochondrial, lipid, and energy metabolism in rats. *PLoS One* 2011; 6: e21779.
17. Cadenas E and Boveris A. Enhancement of hydrogen peroxide formation by protophores and ionophores in antimycin-supplemented mitochondria. *Biochem J* 1980; 188: 31–37.
18. Boveris A, Costa LE, Cadenas E, et al. Regulation of mitochondrial respiration by adenosine diphosphate, oxygen, and nitric oxide. *Methods Enzymol* 1999; 301: 188–198.
19. Boveris A. Determination of the production of superoxide radicals and hydrogen peroxide in mitochondria. *Methods Enzymol* 1984; 105: 429–435.
20. Yagi K. A simple fluorometric assay for lipoperoxide in blood plasma. *Biochem Med* 1976; 15: 212–216.
21. Brand MD and Nicholls DG. Assessing mitochondrial dysfunction in cells. *Biochem J* 2011; 435: 297–312.
22. Kauppinen RA and Nicholls DG. Synaptosomal bioenergetics. The role of glycolysis, pyruvate oxidation and responses to hypoglycaemia. *Eur J Biochem* 1986; 158: 159–165.
23. Choi SW, Gerencser AA and Nicholls DG. Bioenergetic analysis of isolated cerebrocortical nerve terminals on a

microgram scale: spare respiratory capacity and stochastic mitochondrial failure. *J Neurochem* 2009; 109: 1179–1191.
24. Papa S, Francavilla A, Paradies G, et al. The transport of pyruvate in rat liver mitochondria. *FEBS Lett* 1971; 12: 285–288.
25. Reddy PH and Beal MF. Amyloid beta, mitochondrial dysfunction and synaptic damage: implications for cognitive decline in aging and Alzheimer's disease. *Trends Mol Med* 2008; 14: 45–53.
26. Wu JJ, Quijano C, Chen E, et al. Mitochondrial dysfunction and oxidative stress mediate the physiological impairment induced by the disruption of autophagy. *Aging* 2009; 1: 425–437.
27. Tsukada H. The use of (1)(8)F-BCPP-EF as a PET probe for complex I activity in the brain. *Methods Enzymol* 2014; 547: 417–431.
28. Gibson GE, Sheu KF, Blass JP, et al. Reduced activities of thiamine-dependent enzymes in the brains and peripheral tissues of patients with Alzheimer's disease. *Arch Neurol* 1988; 45: 836–840.
29. Almeida CG, Tampellini D, Takahashi RH, et al. Beta-amyloid accumulation in APP mutant neurons reduces PSD-95 and GluR1 in synapses. *Neurobiol Dis* 2005; 20: 187–198.
30. Perez-Nievas BG, Stein TD, Tai HC, et al. Dissecting phenotypic traits linked to human resilience to Alzheimer's pathology. *Brain* 2013; 136: 2510–2526.
31. Ohwada K, Takeda H, Yamazaki M, et al. Pyrroloquinoline Quinone (PQQ) Prevents Cognitive Deficit Caused by Oxidative Stress in Rats. *J Clin Biochem Nutr* 2008; 42: 29–34.
32. Whishaw IQ, Metz GA, Kolb B, et al. Accelerated nervous system development contributes to behavioral efficiency in the laboratory mouse: A behavioral review and theoretical proposal. *Dev Psychobiol* 2001; 39: 151–170.
33. Do Carmo S and Cuello AC. Modeling Alzheimer's disease in transgenic rats. *Mol Neurodegener* 2013; 8: 37.
34. Carreras MC, Franco MC, Peralta JG, et al. Nitric oxide, complex I, and the modulation of mitochondrial reactive species in biology and disease. *Molecul Aspect Med* 2004; 25: 125–139.
35. Moreno-Lastres D, Fontanesi F, Garcia-Consuegra I, et al. Mitochondrial complex I plays an essential role in human respirasome assembly. *Cell Metab* 2012; 15: 324–335.
36. Gabbita SP, Lovell MA and Markesbery WR. Increased nuclear DNA oxidation in the brain in Alzheimer's disease. *J Neurochem* 1998; 71: 2034–2040.
37. Halliwell B and Dizdaroglu M. The measurement of oxidative damage to DNA by HPLC and GC/MS techniques. *Free Radical Res Commun* 1992; 16: 75–87.
38. Nicholls DG. Oxidative stress and energy crises in neuronal dysfunction. *Ann N Y Acad Sci* 2008; 1147: 53–60.
39. Bolanos JP, Almeida A and Moncada S. Glycolysis: a bioenergetic or a survival pathway? *Trends Biochem Sci* 2010; 35: 145–149.
40. Soucek T, Cumming R, Dargusch R, et al. The regulation of glucose metabolism by HIF-1 mediates a neuroprotective response to amyloid beta peptide. *Neuron* 2003; 39: 43–56.
41. Chandrasekaran K, Hatanpaa K, Brady DR, et al. Evidence for physiological down-regulation of brain oxidative phosphorylation in Alzheimer's disease. *Exp Neurol* 1996; 142: 80–88.
42. Dumont M, Ho DJ, Calingasan NY, et al. Mitochondrial dihydrolipoyl succinyltransferase deficiency accelerates amyloid pathology and memory deficit in a transgenic mouse model of amyloid deposition. *Free Radic Biol Med* 2009; 47: 1019–1027.
43. Austin S and St-Pierre J. PGC1alpha and mitochondrial metabolism – emerging concepts and relevance in ageing and neurodegenerative disorders. *J Cell Sci* 2012; 125: 4963–4971.
44. Scheff SW, Neltner JH and Nelson PT. Is synaptic loss a unique hallmark of Alzheimer's disease?. *Biochem Pharmacol* 2014; 88: 517–528.
45. Pathak D, Shields LY, Mendelsohn BA, et al. The role of mitochondrially derived ATP in synaptic vesicle recycling. *J Biol Chem* 2015; 290: 22325–22336.
46. Murthy VN and De Camilli P. Cell biology of the presynaptic terminal. *Annu Rev Neurosci* 2003; 26: 701–728.
47. Tu S, Okamoto S, Lipton SA, et al. Oligomeric Abeta-induced synaptic dysfunction in Alzheimer's disease. *Mol Neurodegener* 2014; 9: 48.
48. Qi Y, Klyubin I, Harney SC, et al. Longitudinal testing of hippocampal plasticity reveals the onset and maintenance of endogenous human Ass-induced synaptic dysfunction in individual freely behaving pre-plaque transgenic rats: Rapid reversal by anti-Ass agents. *Acta Neuropathologica Commun* 2014; 2: 175.
49. Merlini M, Meyer EP, Ulmann-Schuler A, et al. Vascular beta-amyloid and early astrocyte alterations impair cerebrovascular function and cerebral metabolism in transgenic arcAbeta mice. *Acta Neuropathol* 2011; 122: 293–311.
50. Winkler EA, Nishida Y, Sagare AP, et al. GLUT1 reductions exacerbate Alzheimer's disease vasculo-neuronal dysfunction and degeneration. *Nat Neurosci* 2015; 18: 521–530.
51. Takatsu H, Owada K, Abe K, et al. Effect of vitamin E on learning and memory deficit in aged rats. *J Nutr Sci Vitaminol* 2009; 55: 389–393.
52. Zhao L, Gong N, Liu M, et al. Beneficial synergistic effects of microdose lithium with pyrroloquinoline quinone in an Alzheimer's disease mouse model. *Neurobiol Aging* 2014; 35: 2736–2745.
53. Aizenman E, Hartnett KA, Zhong C, et al. Interaction of the putative essential nutrient pyrroloquinoline quinone with the N-methyl-D-aspartate receptor redox modulatory site. *J Neurosci* 1992; 12: 2362–2369.